

# The SKA Galactic Centre Survey

## A White Paper

Rainer Schödel<sup>1</sup>, Antxón Alberdi<sup>1</sup>, Izaskun Jiménez-Serra<sup>2</sup>, Farhad Yusef-Zadeh<sup>3</sup>, Angela Gardini<sup>1</sup>, Michael Kramer<sup>4</sup>, Miguel Pérez-Torres<sup>1</sup>, Mark R. Morris<sup>5</sup>, Jan Forbrich<sup>6</sup>, Adriano Ingallinera<sup>7</sup>, Francisco Nogueras-Lara<sup>8</sup>, Jonathan D. Henshaw<sup>9</sup>, Steven N. Longmore<sup>9</sup>, Javier Moldón<sup>1</sup>, Ian Heywood<sup>10,11,12</sup>, Isabella Rammala<sup>4</sup>, Farideh Mazoochi<sup>13</sup>, Fatemeh Tabatabaei<sup>13</sup>, Lourdes Verdes Montenegro<sup>1</sup>, and Susana Sánchez Expósito<sup>1</sup>

<sup>1</sup>Instituto de Astrofísica de Andalucía (CSIC), Granada, Spain

<sup>2</sup>Centro de Astrobiología (CAB), CSIC-INTA, Torrejón de Ardoz, Spain

<sup>3</sup>Northwestern University, Evanston, IL, USA

<sup>4</sup>Max-Planck-Institute for Radio Astronomy, Bonn, Germany

<sup>5</sup>University of California Los Angeles, Los Angeles, CA, USA

<sup>6</sup>University of Hertfordshire, Centre for Astrophysics Research, College Lane, Hatfield AL10 9AB, UK

<sup>7</sup>INAF - Osservatorio Astrofisico di Catania, Catania, Italy

<sup>8</sup>European Southern Observatory (ESO), Garching bei München, Germany

<sup>9</sup>Liverpool John Moores University, Liverpool, UK

<sup>10</sup>University of Oxford, Oxford, UK

<sup>11</sup>Rhodes University, Makhanda, South Africa

<sup>12</sup>South African Radio Astronomy Observatory, South Africa

<sup>13</sup>Institute for Research in Fundamental Sciences (IPM), School of Astronomy, Tehran, Iran

May 29, 2025

## 1 Abstract

With its extreme density of stars and stellar remnants, dense young massive clusters, high specific star formation rate, intense radiation field, high magnetic field strength, and properties of the interstellar medium that resemble those in high redshift galaxies and starbursts, the Galactic Centre is the most extreme environment that we can observe in detail. It is also the only nucleus of a galaxy that we can observe with a resolution of just a few milli parsecs. This makes it a crucial target to understand the physics of galactic nuclei and star formation, as well as the connection between them. It enables studies of a large number of otherwise rare objects, such as extremely massive stars and stellar remnants, at a well-defined distance, thus facilitating the interpretation of their properties. The Galactic Centre has been and is being studied intensively with the most advanced facilities. In this White Paper, we advocate for a large-area, multi-wavelength survey with the Square Kilometre Array of an area of about  $1.25^\circ \times 0.3^\circ$  (180 pc  $\times$  40 pc), centered on the massive black hole Sagittarius A\* and for repeated deep observations of the nuclear star cluster over a decade, which will allow the community to address multiple science problems with a single data set.

## 2 Science Goals

A survey of the Galactic Centre (GC) with the Square Kilometre Array (SKA) will lead to exquisite data on the nearest galaxy nucleus and probe the physics of the Milky Way's most extreme environment in unprecedented detail and sensitivity. It will enable us to address a large number of key science cases, such as:

1. What is the structure and formation history of the GC as revealed by its stellar remnants?
2. Pulsars: How many pulsars are there in the GC and where are they located? Is there a population of millisecond pulsars (MSPs) at the GC that can serve to test General Relativity (GR)? Can the presence of MSPs explain the GC  $\gamma$ -ray excess?

3. Massive stars: What are the properties of the winds of massive main and post-main sequence stars? Is the current day Initial Mass Function (IMF) at the GC different than in the Galactic disk?
4. What is the present-day star-formation rate at the GC?
5. Can the "building blocks" of life form in GC molecular clouds? How complex can chemistry become in the GC?
6. What are the properties and physics of the large-scale magnetic field in the GC?
7. What is the origin of the magnetised radio filaments in the GC?
8. What is the activity cycle of accreting Neutron Stars (NSs) and Black Holes (BHs) in binaries? Can we improve on our understanding of the radio-near infrared emission correlation in Low Mass X-ray Binaries (LMXBs)? What is the mass function of NSs and BHs in the GC? (This science question will require follow-up observations with extremely large optical telescopes.)
9. Can we confirm or exclude the presence of Intermediate Mass Black Holes (IMBHs) at the GC?
10. What are the properties of infrared extinction towards the GC?

Before discussing these science questions more in detail, we will give a brief summary of our current knowledge about galactic nuclei and about the centre of the Milky Way.

### 3 The nuclei of galaxies

Supermassive BHs (SMBHs) with masses of  $10^{6-8} M_{\odot}$  lie at the photometric and kinematic centres of all major galaxies (see review by [Kormendy & Ho 2013](#)). In addition, Nuclear Star Clusters (NSCs) are present at the centres of practically all galaxies with stellar masses  $> 10^8 M_{\odot}$ . With masses of a few  $10^{5-7} M_{\odot}$  and half-mass radii of a few parsecs, NSCs are the densest stellar systems in the local Universe. The growth and possibly even the formation of massive BHs is linked to the NSCs in which they live (see review by [Neumayer et al. 2020](#)). Interactions between the stars in NSCs and central BHs can give rise to phenomena such as tidal disruption events and gravitational wave emission from inspiral events ([Alexander 2017](#)). Finally, Nuclear Stellar Discs (NSDs), dynamically cold (i.e. flat) rotating stellar systems with radii of a few 100 pc, have been found to surround the NSCs in barred spiral galaxies (see [Gadotti et al. 2020](#)). In these galaxies, Central Molecular Zones (CMZs) are a natural consequence of the inward transport of material towards the nucleus driven by the galactic bar. This influx of gas provides the fuel for star formation that forms nuclear stellar discs and rings.

Galactic nuclei are the most extreme environments in the local Universe. The stellar population in nuclei has been found to be the most metal rich of their host galaxies, with mean metallicities reaching twice solar or higher ([Bittner et al. 2020](#); [Schultheis et al. 2021](#); [Nogueras-Lara 2022](#)). Galactic nuclei thus contain stellar structures and populations that are distinct in their properties and formation histories from the surrounding galactic disc and bars or bulges. Moreover, the Interstellar Medium (ISM) in galaxy nuclei in the local Universe is dense, warm and turbulent, more similar to the conditions found in starbursts and high-redshift star-forming regions than those found in  $z = 0$  galaxy discs. (e.g. [Kruijssen & Longmore 2013](#); [Levy et al. 2022](#)). Galactic nuclei are therefore of fundamental interest for astrophysics.

### 4 The nucleus of the Milky Way

The Milky Way is typical for large spiral galaxies in present-day low density environments ([Bland-Hawthorn & Gerhard 2016](#)). It is a barred spiral with little evidence for any classical, spherical bulge, which is probably due to its quiescent merger history: All five of the up-to-now identified significant merger events had stellar mass ratios smaller than 1 : 31 and occurred  $> 8$  Gyr ago, with the exception of the still ongoing Sagittarius merger (see [Kruijssen et al. 2020](#)).

The Milky Way plays a key role for astrophysics because it provides us with the observational base for the vast majority of astrophysical phenomena at the highest possible linear resolution and at the greatest sensitivity. In particular, our galaxy is a unique laboratory for understanding the nuclei of late-type galaxies. The inward transport of gas through the Milky Way's bar gives rise to its CMZ, which spans a region about 300 pc across, and where up to 10% of our Galaxy's molecular gas can be found (Fig. 1). The conditions in this region (and in similar regions observed in the nuclei of nearby galaxies such as NGC 253, see [Sakamoto et al. 2011](#); [Martín et al. 2021](#)) are so extreme (in terms of density, magnetic fields, turbulence, temperature) that the CMZ is our nearest analogue of high-redshift star-forming regions ([Kruijssen & Longmore 2013](#)).

The GC, is located at  $8.25 \pm 0.01$  kpc from Earth ([Gravity Collaboration et al. 2020](#)). It is the only galactic nucleus in which we can examine the properties and dynamics of stars on milli-parsec scales ([Genzel et al. 2010](#); [Schödel et al. 2014b](#)). On scales of tens to hundreds of parsecs, the GC is the most extreme environment in the Milky Way and its most prolific star-forming region. It can serve as a proxy to understand the conditions in CMZs in general (e.g. [Kruijssen et al. 2014](#); [Henshaw et al. 2023](#)) and it is the best laboratory where to test whether key prebiotic precursors of the "building blocks" of



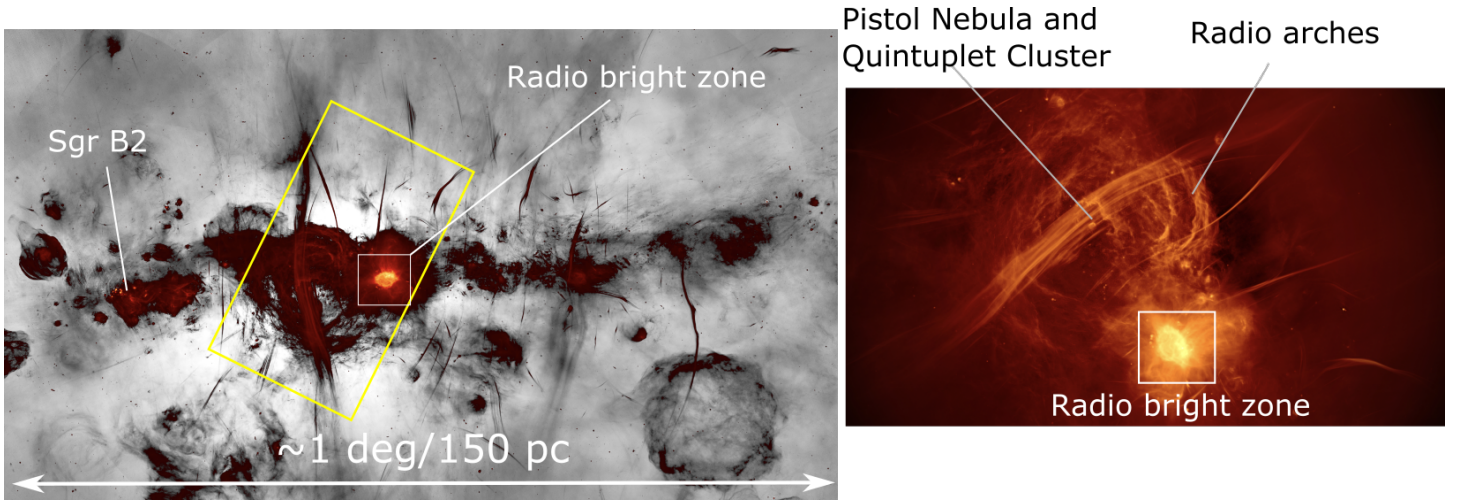


Figure 2: Left: MeerKAT 1.28 GHz image of the GC (Heywood et al. 2022). Galactic north is up, Galactic east is to the left. Right: Zoom into the central area, that is indicated by the yellow rectangle in the left panel.

thermal filaments that can span tens of parsec in length and are estimated to trace a field of  $\sim$ mG strength in the intracloud ISM. The horizontal field is traced by much shorter thermal filaments with field strengths a few tens to a few  $100\mu$ G, that are associated with denser gas and can show signs of deformation by the motion of the ISM.

A final point that needs to be mentioned when discussing the properties of the Milky Way’s nucleus are the formidable observational obstacles. The dusty, molecular clouds along the line-of-sight to the GC cause strong attenuation of electromagnetic radiation in the optical to ultraviolet regime ( $\sim 10^{-12}$  at visible wavelengths). Observations are therefore limited to the radio/mm, infrared, and X/ $\gamma$ -ray regimes. Extreme source crowding requires sub-arcsecond angular resolution to separate its stars and reliably identify counterparts of sources detected at different wavelengths via positional cross-matching. SKA1-Mid will provide us with angular resolutions  $< 0.1''$ . It needs to be complemented by high angular resolution infrared imaging of the region, ideally by NIRCam/JWST (see ?). Meanwhile, our best option is the GALACTICNUCLEUS survey that covers the inner  $0.3\text{ deg}^2$  of the GC with an angular resolution of  $0.2''$  (Nogueras-Lara et al. 2018, 2019).

## 5 The impact of the SKA on GC science

The GC is a prime target for all major telescopes with rich synergies for multi-wavelength studies. This White Paper has a strong emphasis on point-sources, i.e. stars and stellar remnants. In this respect, SKA precursor instruments, such as MeerKAT are limited in their usefulness because of their insufficient angular resolution for the extremely crowded GC (e.g.  $\sim 5''$  in the case of MeerKAT at 1.28 GHz). At the frequencies that we consider here, SKA1-Mid will provide us with a  $\gtrsim 10$  times higher angular resolution at a significantly increased sensitivity (see Tab. 1) and will therefore enable a deep radio survey of a large field as well as repeated surveys of selected pointings for time-domain science and deep studies. The overall structure of the GC as seen in the radio regime is shown in Fig. 2.

Band	Central frequency [GHz]	Beam	Continuum sensitivity [ $\mu$ Jy]
2	1.355	$0.613'' \times 0.600''$	4.47
5a	6.55	$0.127'' \times 0.124''$	0.74
5b	11.85	$0.070'' \times 0.069''$	0.85

Table 1: Beam size and sensitivity of the SKA1-Mid in bands 2, 5a, and 5b. Estimated based on the SKAO Sensitivity Calculator, assuming subarray configuration AA4 (15m antennas only), default bandwidths and central frequencies, 1 h of on-source integration time, and Briggs weighting (Robust setting 0).

We continue to describe the key science cases and how SKA will impact them in more detail.

### 5.1 Stellar remnants and the structure and formation history of the GC

The NSC and NSD can provide us with a proxy for the accretion history of the Milky Way’s nucleus and thus about its evolution and probably also the growth of Sgr A\* (e.g. Neumayer et al. 2020; Nogueras-Lara et al. 2020a; Schultheis et al.

2021; Schödel et al. 2020; Sormani et al. 2022). It appears that both the NSC and the NSD formed very early in our galaxy’s history, at least 8 – 10 Gyr ago (Nogueras-Lara et al. 2020a; Schödel et al. 2020; Sanders et al. 2022). Their high masses and old ages imply the existence of large numbers of stellar remnants. Stellar remnants, in particular NSs and BHs, can provide us with a window into past *massive* star formation and stellar dynamics, i.e. the formation of binaries that contain BHs or NSs. We can expect a large population of LMXBs to form in the dense GC environment, because the relevant tidal capture mechanisms depend on the square of the stellar density (Voss & Gilfanov 2007).

When LMXBs undergo transient accretion activity, they can be detected via their X-ray emission (see Muno et al. 2005; Hailey et al. 2018). X-ray observations need to be carried out from space, which makes them expensive. Also, they provide an angular resolution of at best 0.5'' (with the Chandra X-ray observatory), which makes it challenging to pin down the precise location of sources and thus their potential stellar counterparts. Fortunately, there is a tight correlation between X-ray and radio activity in LMXBs (e.g. Russell et al. 2006; Corbel et al. 2013; Gallo et al. 2018), which makes radio observations an attractive option to infer the number and precise location of stellar remnants in the GC. With its great sensitivity, the SKA will be able to detect LMXBs even in rather faint states. Moreover, the SKA will provide the opportunity to revisit these stellar remnants along their accretion activity cycle.

	WDs	NSs	BHs
NSD	$7.2 \times 10^7$	$3.5 \times 10^6$	$1.8 \times 10^6$
NSC	$2.6 \times 10^6$	$1.3 \times 10^5$	$6.3 \times 10^4$

Table 2: Estimated number of stellar remnants in NSC and NSD.

We can obtain estimates of the number of stellar remnants in the GC by assuming the star formation histories of Nogueras-Lara et al. (2020a) for the NSD and of Schödel et al. (2020) for the NSC <sup>1</sup>. Table 2 lists the estimated numbers of stellar remnants in the NSC and NSD. Different assumptions, such as the number of star formation epochs, the uncertainties in the originally formed stellar mass in each epoch, the metallicity, or initial-to-final mass ratios, may result in changes by up to a few tens of percent, but will not impact the overall magnitude of the numbers. Assuming a homogeneous distribution of the remnants throughout the NSC and an approximate half-mass radius of 4 pc (1 pc corresponds to about 25'' at the distance of the GC), a pencil-beam towards the NSC with a radius of 1.0' may contain of the order of 15000 NSs, 7000 BHs, and  $3 \times 10^5$  White Dwarfs (WDs). These are conservative estimates, because the remnants are not expected to be uniformly distributed, but mass segregated, with stellar BHs, in particular, significantly more concentrated towards Sgr A\* (see Morris 1993; Baumgardt et al. 2018; Hailey et al. 2018; Zhao et al. 2022). Even though we have not considered formation and evolution mechanisms of LMXBs here (which would go far beyond the purpose of this White Paper), these basic considerations illustrate how this large population of stellar remnants offers a great opportunity to constrain the properties of these sources and the structure and star formation history of the NSC and NSD.

The black hole low mass X-ray binary (BHLMXB) GX 339-4 is one of the best-studied sources of its kind. Like the GC, it is located at a distance of about 8 kpc. Its faintest and brightest observed radio luminosities lie between 0.05 and 200 mJy (Corbel et al. 2013), corresponding to a change of about 5 orders of magnitude in its X-ray luminosity. The faintest reported observed radio flux of objects such as GX 339-4 will therefore be accessible with the SKA1-Mid at high significance. Neutron Star Low Mass X-ray Binaries (NSLMXBs) behave in a similar way as BHLMXBs, but display, on average, about 20 times lower luminosity. This still implies that their faint hard states will be observable at the GC with the SKA1-Mid in 1 h-long integrations (Fig. 4). In this context it is also interesting to point out the very faint and ultra-faint X-ray Binaries (XBs) detected at the GC and the possibility that NSLMXBs may have recurrence times of decades between outbursts, much longer than often assumed (Degenaar et al. 2012, 2015; Maccarone et al. 2022), which would imply that many of them may still not have been detected at the GC. Current X-ray transient surveys are limited to luminosities  $\gtrsim 1 \times 10^{34}$  erg s<sup>-1</sup>, corresponding to a few tens of  $\mu$ Jy at  $\sim 10$  GHz for a BHLMXB located at the GC. With a  $3\sigma$  sensitivity around  $2.4 \mu$ Jy in 1 h of observation at 11.85 GHz, the discovery space of the SKA1-Mid will therefore be large: by pushing one order of magnitude deeper in the radio regime we can detect  $\sim 40$  times lower X-ray luminosities.

<sup>1</sup>We approximate the respective star formation histories with four single-age populations: (1) NSD: 90% 8 Gyr, 5% 1 Gyr, 4% 250 Myr, and 1% 40 Myr, where the percentages refer to the originally formed stellar mass at the given age (not to the stellar mass still existing, which is lower). For its total mass we assume  $7 \times 10^8 M_{\odot}$  (Sormani et al. 2020). (2) NSC: 80% 10 Gyr, 15% 3 Gyr, 4% 200 Myr, and 1% 20 Myr. For its total mass we assume  $2.5 \times 10^7 M_{\odot}$  (Schödel et al. 2014a). Variations in the exact ages will not affect in any significant way the number of NSs or stellar BHs, and only to a small degree the number of white dwarfs (WDs). We used the Stellar Population Interface for Stellar Evolution and Atmospheres (SPISEA) Python package (Hosek et al. 2020) to simulate the stellar populations and obtain the number of stellar remnants. We assumed twice-solar metallicity (for metallicities in the GC, see, for example Rich et al. 2017; Nandakumar et al. 2018; Nogueras-Lara et al. 2020a; Schödel et al. 2020; Schultheis et al. 2021). We used the *IFMR\_Raithe18* class to assign initial-to-final mass ratios. The fractions of NSs and BHs originally formed in multiples is  $\geq 0.99$  and those of WDs formed in multiples is  $\sim 0.5$ . For lack of any further information we assumed a power-law IMF constant with time (exponent  $-2.3$  between 0.5 and 120  $M_{\odot}$ ,  $-1.3$  for smaller masses). Pfuhl et al. (2011) find no evidence for a significantly altered IMF in the past. There is, however, significant evidence for a top-heavy IMF in the star formation event that created on the order of 200 massive stars within 0.5 pc of Sgr A\* about 4 million years ago (see e.g. Bartko et al. 2010; Lu et al. 2013). Our estimate of the number of stellar remnants may therefore be conservative.

The radio regime suffers practically no interstellar extinction, contrary to X-rays and the infrared. Observations of LMXBs will be key to address fundamental questions about the structure and evolution of the Milky Way’s nucleus. Since the distribution of LMXBs will follow the underlying stellar density, their observation provides us with a way to determine the shape and symmetry of the NSD and NSC. This is, for example, of great importance for the NSC, because its southern part is hidden by large dark clouds (Schödel et al. 2014b; Gallego-Cano et al. 2020; Zhu et al. 2018). Observations of BHLMXBs will also enable tests of mass segregation in the NSC (e.g. Morris 1993; Zhao et al. 2022). Once we know the distribution of stellar BHs around Sgr A\*, more accurate predictions can be obtained for extreme mass-ratio inspiral events that may be observed in other galaxies with the LISA gravitational wave observatory.

Although it is currently assumed that the NSC and NSD are different structures, they may be related, with a smooth transition between them, as suggested by Nogueras-Lara et al. (2023). The ratio between stellar mass and the number of stellar remnants for the two structures may provide additional constraints on their relation (but the effects of the dynamical formation of XBs may have to be taken into account Generozov et al. 2018).

The number of LMXBs at the GC may be able to constrain whether massive stars formed preferentially at the GC, not just in the most recent star formation event, but also in the past (combined with star formation history and kinematic models; a challenging undertaking).

*State-of-the-art.* Zhao et al. (2022) report on the detection of what they call hyper-compact radio sources in 33.0 and 44.6 GHz JVLA A configuration images of the central 0.8 pc×0.8 pc (20" × 20") of the Milky Way. They define as "hyper-compact" those sources that have a major axis size of < 0.1". After applying strict detection thresholds and requiring that the Ka- and Q-band positions must have a relative positional offset < 3σ, they identify 64 such sources. A large sub-sample of 38 of those sources (58%) have steep spectra,  $S_\nu \propto \nu^\alpha$  with  $\alpha = -1.8 \pm 0.2$ . These are probably associated with LMXBs and are strongly concentrated towards the central SMBH, as expected from theory and in agreement with X-ray observations (Morris 1993; Muno et al. 2005; Hailey et al. 2018; Generozov et al. 2018; Zhao et al. 2022).

*Impact of the SKA.* SKA1-Mid will be able to reach angular resolutions of 0.13" and 0.07" at 6.55 and 11.85 GHz with an rms noise of 0.7 – 0.8 μJy beam<sup>-1</sup> in 1 h integrations. At 11.85 GHz its angular resolution is comparable to the one of the JVLA at 33 GHz, but with a much rounder beam, given the southern location of the GC. In addition, the high angular resolution of the SKA1-Mid will be available at a significantly lower frequency, which favours the detection of the type of steep-spectrum sources that are probably associated with massive stellar remnants (synchrotron emission). A more general discussion of the impact of SKA on the study of stellar remnants can be found in Corbel et al. (2015).

## 5.2 Pulsars

Pulsars serve, among others, to perform fundamental tests of physics (Kramer 2016). The study of radio pulsars at the GC is one of the central SKA science cases, because we expect a large number of them in this region and thus a high probability of finding double-pulsars or a pulsar in orbit around a stellar BH. A pulsar may even be present in a tight orbit around Sgr A\*. Both scenarios would provide an exquisite probe of the physics of gravity (Kramer et al. 2004; Eatough et al. 2015). Even though the probability of observing a normal pulsar (NP) on a short period (~1 yr) orbit around Sgr A\* that is beamed towards Earth may be rather low (Schödel et al. 2020), the intense star-formation activity in the GC in the past ~10 Myr suggests the presence of (up to a few) 100 pulsars throughout the central parsec (Eatough et al. 2015; Schödel et al. 2020). About 20% of them may be beamed towards Earth.

Apart from NPs, which are young NSs with spin periods of one to a few 0.1 – 1 s there exist the so-called *MSPs*, old NSs spun up to reach fast rotational periods by accretion from a stellar companion. Given the old age of the stellar population in the GC as well as the large stellar density, such pairs of NSs and donor stars may form dynamically in close encounters. MSPs are of great interest, because they can serve to obtain extremely accurate dynamics, and therefore insights on the structure and dynamics of the GC. If they are found near Sgr A\* or orbiting a stellar BH, they can be exquisite probes of GR/theories of gravity. This is actually true for any pulsar in a sufficiently compact orbit, which is hence a strong motivation to search for pulsars in the GC (Liu et al. 2012; Psaltis et al. 2016).

The detection of pulsars in the GC would also enable detailed studies of the ISM structure through spatial analysis of scattering screens (Bower et al. 2014).

Surprisingly, to this day only seven pulsars have been detected in the GC region, which we define in this paper to be the region inside the CMZ (see sec. 4). Six of these pulsars all lie at projected distances  $R > 10'$  ( $R > 24$  pc) from Sgr A\* (Deneva et al. 2009; Schnitzeler et al. 2016; Wongphechauxsorn et al. 2024). The magnetar is at  $R \sim 2.5''$  ( $R \sim 0.1$  pc).

This so-called *missing pulsar problem* is a key puzzle of GC astrophysics (e.g. Torne et al. 2021). A possible explanation may be the challenge to observe pulsars in this environment: Typically, pulsars and magnetars are identified by their pulses, but scatter broadening makes this task difficult at the GC (e.g. Eatough et al. 2015; Torne et al. 2021). There may also exist deeper astrophysical reasons that could explain the dearth of pulsars. Dexter & O’Leary (2014) and Zhao et al. (2022), for example, discuss the intriguing hypothesis that most NPs may be born as magnetars in the GC. Since the spin-down time of magnetars is much shorter than the one of NPs, this hypothesis could explain the missing pulsars problem at the GC.

The GC γ-ray excess was discovered by Fermi/LAT more than a decade ago (Hooper & Goodenough 2011). It is of great interest for fundamental physics, because it may be caused by the self-annihilation of dark matter particles at the GC (e.g. Salati 2014). An alternative explanation for this excess of GeV radiation is the presence of a substantial population of MSPs

at the GC (e.g. [Abazajian 2011](#)). With the SKA we will be able to test this hypothesis with sufficiently deep observations and thus be able to settle a long-standing question.

*State-of-the-art.* To this date, seven pulsars have been confirmed in the GC, three of which appear to be magnetars ([Wong-phechauxsorn et al. 2024](#)). As concerns the search for candidates, ([Zhao et al. 2020](#)) analysed multi-epoch JVLA data at 5.5 GHz. They report the detection of 110 compact sources (size  $< 1''$ ). They estimate mean flux densities of  $50 \mu\text{Jy}$  for NPs and  $5 \mu\text{Jy}$  for MSPs at the distance of the GC. From their analysis (based on the observed luminosity function and non-variability on a timescale of 6 years) we can infer that on the order 20 of their sources are potential NPs.

[Zhao et al. \(2022\)](#) analysed 33.0 and 44.6 GHz JVLA A configuration images of the central  $0.8 \text{ pc} \times 0.8 \text{ pc}$  ( $20'' \times 20''$ ) of the Milky Way. They reach an angular resolution of  $\sim 0.05''$  and an rms noise of 17 and  $8 \mu\text{Jy beam}^{-1}$  at 33 and 44 GHz. They discover a small number (15%) of flat-spectrum hyper-compact regions, which may be unresolved peaks of the ISM in complex mini-spiral HII region. About a quarter of their detections, 26%, have inverted spectra, which rise towards higher frequencies. Even though a large fraction of the sources with inverted spectra are probably related to stellar winds around massive stars, [Zhao et al. \(2022\)](#) speculate, based on their study of the spectrum of the magnetar SGR J1745–2900, that some of the inverted-spectrum sources may be magnetars.

*Impact of the SKA.* SKA will be instrumental in finding pulsars at the GC. SKA1-Mid is expected to reach a continuum rms noise of 5.3, 0.7, and  $0.8 \mu\text{Jy beam}^{-1}$  at 1.355, 6.55, and 11.85 GHz in one-hour-long integrations. Assuming  $S_\nu \propto \nu^\alpha$  and a spectral index of  $\alpha = -1.6$  ([Jankowski et al. 2018](#)), NPs will have mean flux densities of about  $510 \mu\text{Jy}$  at 1.4 GHz,  $40 \mu\text{Jy}$  at 6.7 GHz, and  $12 \mu\text{Jy}$  at 12.5 GHz at the distance of GC. The corresponding values for MSPs will be  $51 \mu\text{Jy}$  at 1.4 GHz,  $4 \mu\text{Jy}$  at 6.7 GHz, and  $1.2 \mu\text{Jy}$  at 12.5 GHz. Hence, at 6.7 GHz the SKA will supersede the previously mentioned 5.5 GHz JVLA observations by a factor of roughly five in sensitivity and angular resolution. If we assume a spectral index of  $\alpha = 0.6$  for the inverted-spectrum radio sources (hypothetical magnetars), then SKA1-Mid will still be about five times more sensitive at 11.85 GHz than the JVLA at 33.0 GHz, while also providing a rounder beam at an equivalent angular resolution. MeerKAT is evolving rapidly and is already superseding the JVLA in sensitivity at low frequencies, but is limited in its high frequency capabilities.

In 10 h of observation, an rms noise of  $\sim 0.2 \mu\text{Jy beam}^{-1}$  can be reached at 6.7 GHz, which implies the possibility to detect MSPs at the  $7\sigma$  level with SKA1-Mid. Follow-up pulsar-timing, multi-wavelength and polarisation observations will be essential for confirming the nature of the sources and potentially identifying magnetars via their spectral properties (see next section).

With the help of VLBI observations, which will profit significantly from the inclusion of SKA1-Mid, we will be able to measure the proper motions of NPs at the GC (see [Bower et al. 2015](#)), which can provide us with upper limits on how deep they are located inside the potential of Sgr A\*. Finally, in 100 h, e.g. from stacking ten epochs of 10 h observations, MSPs can be detected in all three bands with a significance of  $> 10\sigma$ , but interstellar scattering may prevent identifying their pulses. Assuming scattering as observed for the GC magnetar (see e.g. [Spitler et al. 2014](#)), observing frequencies above 30 GHz may be needed.

### 5.3 Massive stars, their winds and the IMF at the GC

Averaged by volume, the GC is the Milky Way’s most prolific star-forming region. It contains a large number of massive stars, for example in the central parsec, in the Arches and Quintuplet clusters, as well as distributed throughout the NSD (see [Clark et al. 2021](#)). Since all these stars are located at a well-known, well-defined distance, the GC is a convenient laboratory where we can study the still poorly known evolution of massive stars, in particular their mass loss.

Obtaining an accurate census of young, massive stars at the GC is highly challenging, because of extreme interstellar extinction and stellar crowding (see [Schödel et al. 2014b](#)). Massive post-main-sequence stars have been detected via narrow-band infrared, radio, and X-ray observations all over the GC (e.g. [Mauerhan et al. 2010](#); [Dong et al. 2011](#)). However, existing observations have incomplete coverage of the GC, have not been performed systematically, and would have missed O-main-sequence stars. An alternative way to find young, massive stars is to identify them via the emission from their strong, ionised winds and, possibly, circumstellar nebulae (depending on their evolutionary state). Thus, SKA can help to constrain recent star formation at the GC and study mass loss via stellar winds and circumstellar nebulae (e.g. Pistol star near the Quintuplet cluster, [Lang et al. 2005](#)).

*State-of-the-art.* [Gallego-Calvente et al. \(2021\)](#) and [Gallego-Calvente et al. \(2022\)](#) observed the Arches and Quintuplet massive young clusters at the GC (located at about 25 pc or 10 arcmin in projection from Sgr A\*) with the A configuration of the JVLA at 6 and 10 GHz, reaching an rms noise of about  $9 \mu\text{Jy beam}^{-1}$  at 6 GHz and  $5 \mu\text{Jy beam}^{-1}$  at 10 GHz, with an angular resolution of  $\sim 0.5''$ . They correlate the discovered compact sources with young massive stars detected in the near-infrared and report the detection of 18 radio sources associated with massive stars in the Arches cluster and 29 in the Quintuplet cluster, thus increasing the detected number of such stars in these clusters by factors two to three. [Gallego-Calvente et al. \(2022\)](#) also use the data to derive mass loss rates, identify potential binaries and study the mass loss rate variability by comparing observations at two different epochs. Remarkably, they find that the observed numbers of radio stars imply a non-standard, top-heavy or bottom-light initial mass function in both clusters (as compared to the typical Salpeter or Kroupa IMF found in other regions of the Milky Way), in agreement with what has been found in near-infrared observations ([Hußmann et al. 2012](#); [Hosek et al. 2019](#)).

*Impact of the SKA.* Due to the inverted spectrum of the radio emission from stellar winds, the SKA1-Mid, with its lower frequency receivers, will provide us with only a moderate improvement in sensitivity for the study of radio stars, compared to non-thermal sources. However, its significantly higher angular resolution (about a factor of 5) will allow us to disentangle massive stars in high-density regions such as Arches, Quintuplet or central parsec, and to obtain significantly better astrometry for kinematic measurements. With 10 h long observations at 12.5 GHz, SKA1-Mid can reach an rms noise as low as  $0.4 \mu\text{Jy beam}^{-1}$  and thus detect winds from all massive post-main-sequence stars and from main-sequence O-stars down to about  $30 M_{\odot}$  in the GC, and provide us with a more complete picture of recent (very) massive star formation at the GC. It will also allow us to study the wind mass loss from hundreds of stars that are located at a well determined distance, thus providing a firm footing for studies of stellar-wind mass loss. Note that SKA1-Mid will simultaneously observe several hydrogen radio recombination lines together with the continuum emission, which will be used to constrain the internal physical structure and kinematics of massive stellar winds by means of 3D radiative transfer modeling (using the M<sub>O</sub>d<sub>E</sub>l for REcombination L<sub>I</sub>nes or MORELI code; Baez-Rubio et al. 2014; Martinez-Henares et al. 2023). This will allow us to investigate the launching mechanisms as well as the physical properties of the winds (mass, momentum, and energy) in a statistically relevant sample.

SKA1-Mid will also provide stronger constraints on the mass function of massive stars in the GC than what has been possible until now. It should be noted that the combination of short and long uv spacings with the SKA observations will facilitate the imaging of both extended and compact emission simultaneously, allowing the detection of point sources even within the diffuse emission (synchrotron or thermal free-free emission from star-forming regions), which would not be possible with other instruments.

Figure 3 shows the potential impact of studying the radio luminosity function of a region containing young stars. As an example we use the Sgr B1 region in the GC. It was recently reported that Sgr B1 contains about  $10^5 M_{\odot}$  of massive stars that formed roughly 10 Myr ago (Nogueras-Lara et al. 2022). Massive stars develop intense stellar winds once they turn off the main sequence. These winds give rise to thermal radio emission (with possible non-thermal contributions from colliding wind binaries). Radio emitting stars can be easily identified and distinguished from other radio sources by their necessarily precise astrometric coincidence with infrared-bright stars. With radio continuum observations we can measure the radio luminosity function of massive stars in a region such as Sgr B1. The radio luminosity function evolves significantly as a function of age, because it is a function of the rapid evolution of massive stars. Therefore radio continuum observations with SKA would be able to constrain the age of the star formation event that underlies the young population in HII regions such as Sgr B1.

## 5.4 Present day star formation

In spite of the presence of copious amounts of molecular gas at extremely high densities, the Milky Way appears to be a significant outlier in the empirically derived relations between gas density and star formation activity (see review by Henshaw et al. 2023). One of the main difficulties in constraining the present-day star formation rate is that the extreme opacity of the molecular clouds at the GC may prevent us from detecting a significant fraction of the deeply-embedded young stellar objects. SKA1-Mid will cover a series of rotational lines of cyanopolyynes such as  $\text{HC}_3\text{N}$ ,  $\text{HC}_5\text{N}$ ,  $\text{HC}_7\text{N}$  and  $\text{HC}_9\text{N}$  (see e.g. Bianchi et al. 2023). These molecules are excellent probes of the deeply-embedded population of massive young stellar objects at the hot core stage<sup>2</sup>. Indeed, they are largely enhanced in hot cores by the thermal evaporation of ices from grains as a result of the high temperatures of the dust (Viti et al. 2004; Martín-Pintado et al. 2005).  $\text{HC}_5\text{N}$  is particularly interesting for SKA1-Mid because it presents four rotational lines in the  $v=0$  state lying within bands 5a and 5b. The high-angular resolution of the proposed survey (beam of  $0.07''$  -  $0.13''$ ) will filter out any low-excitation extended emission of  $\text{HC}_5\text{N}$ , pinpointing the location of the high-excitation  $\text{HC}_5\text{N}$  emission arising from hot cores. Therefore, molecular line observations of  $\text{HC}_5\text{N}$  with SKA1-Mid (and, possibly, of even larger cyanopolyynes) will provide a complementary view to the one of the continuum images, giving information about the youngest population of massive stars in the making in the GC.

Last but not least, SKA1-Mid will also be able to probe maser emission from high-mass star formation (including methanol masers in the 6.7 and 12 GHz bands). These would not only be useful to pinpoint such regions of high-mass star formation, but additionally they could serve as a starting point for future SKA-VLBI astrometry and parallax measurements, along the lines of what the BeSSeL survey has provided for the northern sky (e.g., Reid et al. 2014).

*State-of-the-art.* The line emission of  $\text{HC}_3\text{N}$  and  $\text{HC}_5\text{N}$  has recently been imaged across the CMZ within the ALMA Large Program ACES (ALMA CMZ Exploration Survey). This survey, however, has been acquired with an average angular resolution of  $1.5''$ , insufficient to resolve the hot core population whose expected hot core sizes are  $\sim 0.06''$  -  $0.13''$  (or  $\sim 500$  -  $1000$  au at the distance of the GC).

*Impact of the SKA.* SKA1-Mid will cover all rotational lines from  $J=5$  to  $J=2$  in the ground vibrational level of  $\text{HC}_5\text{N}$ .  $\text{HC}_5\text{N}$  is measured to be factors of 2-3 less abundant than  $\text{HC}_3\text{N}$  in GC sources (see Zeng et al. 2018, 2018MNRAS.478.2962Z). For the hot cores of Sgr B2(N), the  $\text{HC}_3\text{N}$  column densities are of  $\sim 10^{17} \text{ cm}^{-2}$  within a beam of  $1''$  (see de Vicente et al. 2000). These column densities are expected to be of  $\sim 10^{19} \text{ cm}^{-2}$  for hot core sizes of  $0.1''$ . Therefore, we can assume a  $\text{HC}_5\text{N}$  column density of  $\sim 3 \times 10^{18} \text{ cm}^{-2}$  for the hot cores in the GC. Using this column density, a linewidth for the  $\text{HC}_5\text{N}$  emission of  $8 \text{ km s}^{-1}$ , and a gas temperature of 300 K (typical of hot cores in the GC; de Vicente et al. 2000), we expect

<sup>2</sup>Hot cores are compact ( $\leq 0.1$  pc), dense ( $\text{H}_2$  volume gas densities  $\geq 10^8 \text{ cm}^{-3}$ ) and hot ( $T \geq 150$ - $300$  K) condensations that represent the cradles of massive stars (Garay & Lizano 1999).

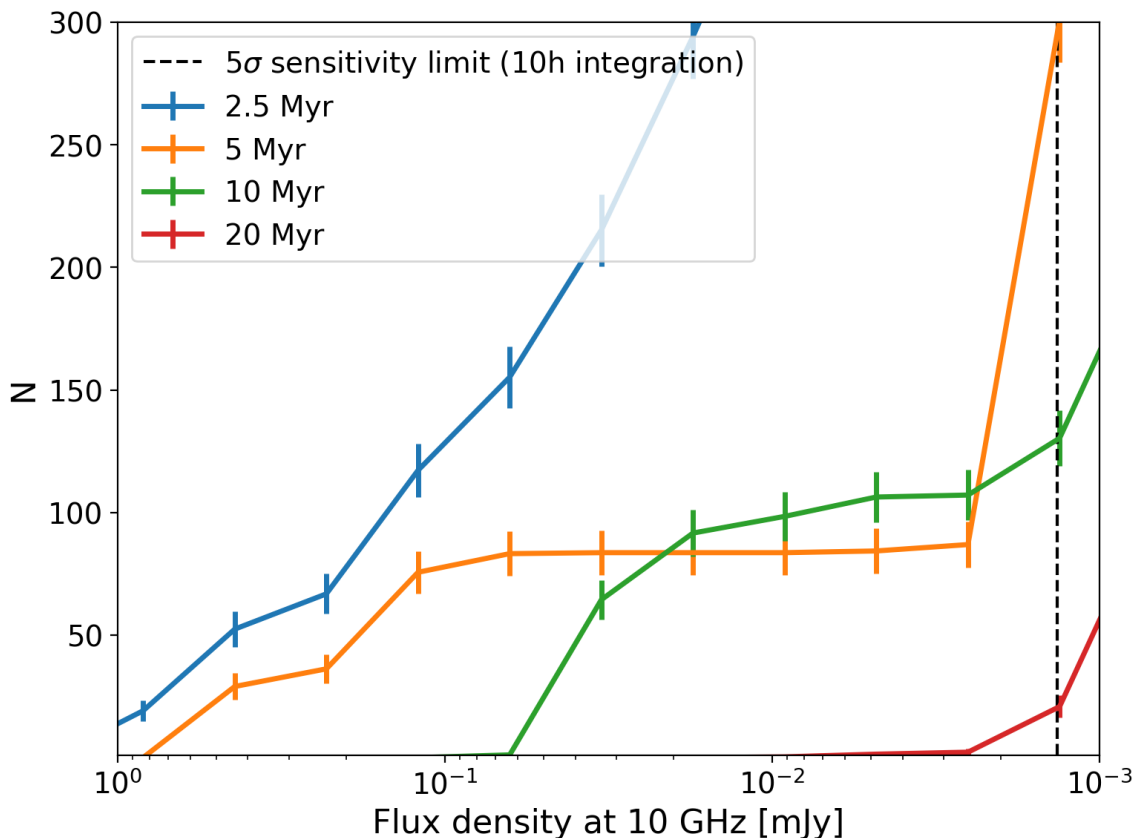


Figure 3: Cumulative radio luminosity functions for a star-forming event of  $10^5 M_{\odot}$  at the distance of the GC and with different assumed ages. Prediction from MIST isochrones, using Monte Carlo simulations to sample the mass function. The mass-loss rates of the stars that are provided by the MIST models were converted to radio luminosities (e.g. [Leitherer et al. 1997](#)). The RLFs have different characteristic shapes at each age, which can allow us to constrain both the age (via the shape of the RLF) and mass (total number) of a star forming event.

peak fluxes for the  $\text{HC}_5\text{N}$  rotational lines of  $\sim 125\text{-}300 \mu\text{Jy}/\text{beam}$ . These lines will be detected with  $S/N > 3\text{-}7$  in integrated intensity, unveiling the population of GC hot cores.

## 5.5 Searching for the “building blocks” of life

The Giant Molecular Clouds in the GC are apparently the most chemically rich repositories of molecular material in our Galaxy (e.g. [Requena-Torres et al. 2008](#)). In the past few years, about two dozen new molecular species have been discovered in the dense clouds in the CMZ. Interestingly, some of these species are of prebiotic interest and include precursors of ribonucleotides, nucleobases, sugars, proto-proteins and proto-lipids (e.g. [Rivilla et al. 2021, 2022, 2023](#); [Rodríguez-Almeida et al. 2021b,a](#); [Zeng et al. 2021](#); [Sanz-Novo et al. 2023](#); [Jiménez-Serra et al. 2020, 2022b](#)). These molecules are better detected in the CMZ because of the large column densities found in GC molecular clouds. Therefore, these clouds represent a unique opportunity to learn about how complex the chemistry of the ISM can become, and whether the building blocks of life could form already in interstellar space.

*State-of-the-art.* All these molecules have been discovered in emission in the 7mm, 3mm and 2mm bands and they likely represent the tip-of-the-iceberg. However, due to the high sensitivity already reached by the single-dish, broadband spectral surveys already carried out with the Yebes 40m and IRAM 30m telescopes, we are starting to reach the line confusion limit in the observed spectra for these objects, which prevents the discovery of new prebiotic species of even higher complexity. The only way to circumvent this problem is to observe these molecules at even lower frequencies, which are much cleaner from simpler and smaller molecules. The problem is that the line transitions of large molecules such as prebiotic species become weaker since their partition functions become large (the population of any given molecule gets spread over a greater number of energy levels). In addition, at low frequencies their Einstein  $A_{ul}$  coefficients become orders of magnitude smaller (typically from  $10^{-6} \text{ s}^{-1}$  to  $10^{-9} \text{ s}^{-1}$ ). This issue is alleviated if we observe these species in absorption against strong background sources instead of in emission ([Jiménez-Serra et al. 2022a](#)).

*Impact of the SKA.* By performing spectroscopic surveys toward strong continuum centimeter sources, SKA1-Mid has the potential to discover new prebiotic interstellar species in absorption spectra. As an example, [Jiménez-Serra et al. \(2022a\)](#) have shown that a few rotational lines from the C3 sugar glyceraldehyde (i.e. a sugar with three carbon atoms) will be

detected with a  $S/N \geq 3$  in integrated intensity with SKA1-Mid in bands 5a and 5b in 1 hour integration time. Larger sugars such as erythrose (a C4 ketose sugar), however, will require hundreds of hours of integration time (Jiménez-Serra et al. 2022a). But the proposed survey will represent a key step for the discovery of large prebiotic molecules because it will reveal the location of the strongest continuum background sources in bands 5a and 5b toward which to carry out future dedicated high-sensitivity spectral surveys with SKA1-Mid.

## 5.6 Properties and physics of the large-scale magnetic field

Among the biggest open questions concerning the GC magnetic field are: (1) Is the milligauss vertical field homogeneous and pervasive throughout the CMZ and does this define an overall GC magnetosphere or are the strongest magnetic features only localised, transient features? (2) How and where does the vertical field couple to the horizontal field? Can we find specific points of interaction? (3) What is the origin of the relativistic electrons that light up the NTFs (see next subsection)? (4) What is the origin of the poloidal field?

Studies of MeerKAT continuum data at 1.3 GHz (e.g. Heywood et al. 2022; Yusef-Zadeh et al. 2023) have traced the thermal and non-thermal filaments with unprecedented sensitivity and have provided an impressive new view of the GC magnetic field. Still, they are limited to an angular resolution  $\simeq 5''$ , which makes it hard to untangle different features and detect faint filaments in the radio bright GC.

The SKA1-Mid in bands 2, 5a, and 5b will provide sensitive, high-resolution radio continuum maps, enabling to study the magnetic field with angular resolutions almost ten times better than the published MeerKAT observations. This will shed light on the role of the magnetic field in the GC on scales down to milli-parsecs. So far undiscovered faint filaments will improve our knowledge of the magnetic field and of the origin of the relativistic electrons that power the NTFs. One particularly important question here is the existence or not of non-thermal horizontal filaments close to the Galactic plane. The data will provide us with a better understanding of the influence of the magnetic field on the dynamics of the ISM, which may even come to dominate some HII regions (see ?). An exciting prospect is that the high angular resolution of SKA-MID may allow us to perform proper motion measurements of magnetic filaments over timespans of a few to ten years. Proper motions could help us clarify the relative locations, interactions and whether the vertical field does or does not rotate with respect to the ISM and stars, which could indicate whether we are seeing global field configurations or whether the NTFs are localised, short-lived features.

## 5.7 Origin of the non-thermal filaments

One of the first hints showing that the nucleus of our Galaxy harboured energetic activity was the discovery of the archetype magnetised radio filaments in the GC 40 years ago (Yusef-Zadeh et al. 1984). Since then, radio observations have shown a population of linearly polarised synchrotron emission tracing nucleus-wide cosmic ray activity throughout the inner few hundred parsecs of the Galaxy (e.g. Heywood et al. 2019). Furthermore,  $H_3^+$  absorption-line measurements of this region determined high cosmic-ray ionisation rates indicating that relativistic particles permeate the CMZ at levels a thousand times that in the solar neighbourhood (Oka et al. 2005; Indriolo & McCall 2012; Le Petit et al. 2016). These particles provide a significant source of pressure in the GC when compared to thermal gas pressure in the ISM of the GC. It is also becoming clear that there is another population of radio filaments detected in radio galaxies in poor clusters. These extragalactic filaments show remarkably similar underlying physics to those of the GC, in spite of vastly different scale lengths and environments (Yusef-Zadeh et al. 2023). The origin of this class of filaments is not understood either (Ramatsoku et al. 2020; Rudnick et al. 2022). However, the similarities provide an opportunity to investigate the physical processes in the ISM of the GC and compare them to the environment of the intracluster medium for the first time using detailed and sensitive SKA observations.

One of the key questions is the origin of the filaments in the GC and in radio galaxies. There is no obvious source that powers these nonthermal filaments. Although numerous models have been proposed to explain the origin of the filaments, there is no consensus how the filaments are produced. One filament origin, known as the cometary model, invokes an energetic compact source, possibly a fast-moving pulsar or a mass-losing stellar wind sources, accelerating cosmic rays to high energies (Yusef-Zadeh & Wardle (2019)). Remarkably, motivated by the search for pulsation from the steep spectra compact source embedded within the snake filament (Yusef-Zadeh et al. 2024), the recent discovery of the first GC MSPs (Lower et al. 2024), likely associated with a filament  $\sim 1$  arcmin from the snake filament (termed "Sunfish" filament by the author), motivates further observations with the SKA to determine if pulsars power nonthermal radio filaments.

A search for compact radio sources associated with nonthermal radio filaments found an initial sample of 46 sources that lie near the ends of filaments using MeerKAT data (Yusef-Zadeh et al. 2023). In the cometary scenario, the filaments result from the collection and draping of magnetic field lines by a moving stellar wind bubble or a pulsar with respect to the medium and forming a cometary tail. The nature of these compact sources and their physical association with the filaments are not clear. The SKA GC survey with its remarkable sensitivity, resolution and broad bandwidth will be able to test this model. In particular, the spectral index of the compact sources will be determined, placing constraints on steep spectrum pulsar candidates and stellar wind sources. In addition, high spatial resolution will provide details of possible interaction of the compact radio sources with the filaments. Lastly, the remarkable sensitivity will be able to uncover fainter filaments

than those detected in the MeerKAT survey of the GC. The brightness distribution of the filaments may have important implications on a process that involves the turbulent environment in which GC filaments are produced.

## 5.8 Stellar remnants: activity cycles, radio-infrared correlation, mass function

Observations of the GC will enable studies of the properties of BH/NSLMXBs with a large sample at a well-known distance. They will allow us to improve significantly our understanding of the infrared-radio-X-ray correlation of LMXBs (Coriat et al. 2009) with parallel infrared observations. Observations repeated over time scales of years will allow us to better constrain the recurrence cycles of BH/NSLMXBs. With repeated observations over about a decade of operations, the SKA will detect hundreds of LMXBs in the NSC and control fields. This will allow us to obtain better constraints on our so far poorly constrained knowledge about the recurrence time of outbursts in XBs.

Russell et al. (2006) and Russell et al. (2007) show that there exists a tight correlation between X-ray and optical/near-infrared emission for BHLMXBs (and probably also NSLXBs). SKA1-Mid can easily detect and follow-up transients at the GC. Near-infrared cameras such as ERIS/VLT can detect the near-infrared counterparts of BHLMXBs almost down to quiescence. This offers the possibility to study the radio-X-ray-infrared correlation of LMXBs (and thus accretion physics) with coordinated observations with high angular resolution near-infrared imaging instruments such as ERIS/VLT and, in particular, MOSAIC/ELT.

SKA1-Mid will allow us to find a highly complete sample of stellar remnants in binary systems at the GC. Those systems may be followed up spectroscopically and astrometrically by the ELT and the VLT interferometer to determine the mass function of the remnants. This can provide us with potentially hundreds of mass measurements in a region with a well defined properties. Since the mean metallicity is high (about twice solar at the GC), we can gain insights how metallicity influences wind mass loss from massive stars and the final mass of stellar BHs.

## 5.9 Extinction towards the GC

Interstellar extinction is extreme and highly variable as a function of the line-of-sight towards the GC (see e.g. Scoville et al. 2003; Nogueras-Lara et al. 2020b). It is one of the greatest obstacles in our interpretation of infrared observations of stars in the GC. For example, accurate and precise measurements of extinction are needed to correct observed stellar magnitudes and thus to be able to classify stars approximately via photometric measurements (e.g. ?). Also, the conversion of observed fluxes to absolute fluxes depends sensitively on an accurate knowledge of extinction, implying an insecurity of a factor of up to two in the estimated stellar masses of young, massive stars (e.g. Clark et al. 2018). Combining measurements of radio hydrogen recombination lines with infrared HI emission lines is a highly reliable way of measuring absolute extinction as a function of wavelength towards the GC (see Scoville et al. 2003; Fritz et al. 2011).

Emission from ionised ISM is pervasive in the GC. SKA observations of radio recombination lines, which are unaffected by extinction, can be combined with infrared recombination lines from NIRCcam/JWST (see ?). Such data would allow us to determine the extinction curve with great accuracy across the GC and test whether and how it depends on the line of sight and on infrared wavelength (see, e.g., discussion in Nogueras-Lara et al. 2021). In addition, knowledge of extinction towards different ISM features will allow us to constrain their relative distances along the line of sight and therefore the 3D-distribution of the ISM at the GC.

## 5.10 IMBHs

There have been speculations on the presence of IMBHs at the GC (e.g. Tsuboi et al. 2017). SKA1-Mid would be sensitive enough to detect all potential IMBH candidates throughout the GC, even when they are in a quiescent state, such as Sgr A\*. Their nature can then be inferred via variability studies, VLBI, and stellar kinematic studies.

# 6 Properties of point-like radio sources at the GC

Figure 4 provides an overview of point-like sources at the GC and their expected flux densities at different frequencies. Apart from their fluxes, the different types of point sources can be distinguished in various ways: Wolf Rayet and O-type main and post main sequence stars will have bright near-infrared counterparts and frequently thermal radio spectra. Pulsars will typically have steep spectra (with the possible exception of magnetars, which may have flat to inverted spectra, see Zhao et al. 2022), polarised emission (Sobey et al. 2022) and show little variability. LMXBs will show great variability with most of them manifesting as transient sources. In the low/hard state they typically show flat to inverted spectra from optically thick jet bases, i.e.  $\alpha > 0$  for  $S_\nu \propto \lambda^\alpha$ , where  $S_\nu$  is the radio flux density and  $\lambda$  the wavelength, but they become optically thin ( $\alpha < 0$ ) in the high/soft state (Fender et al. 2004). As concerns multi-wavelength cross-identification, Ultracompact HII and similar nebular sources have sizes  $\lesssim 0.1$  pc, corresponding to  $\lesssim 2.5''$  at the distance of the GC. Practically all of them will therefore be resolved and/or have an infrared counterpart. Near-infrared imaging with an angular resolution of  $0.2''$  is available from the GALACTICNUCLEUS survey (Nogueras-Lara et al. 2019). Higher angular resolution imaging from JWST NIRCcam has already been obtained on some selected fields (such as the central parsecs, Sgr C, or the Brick molecular cloud)

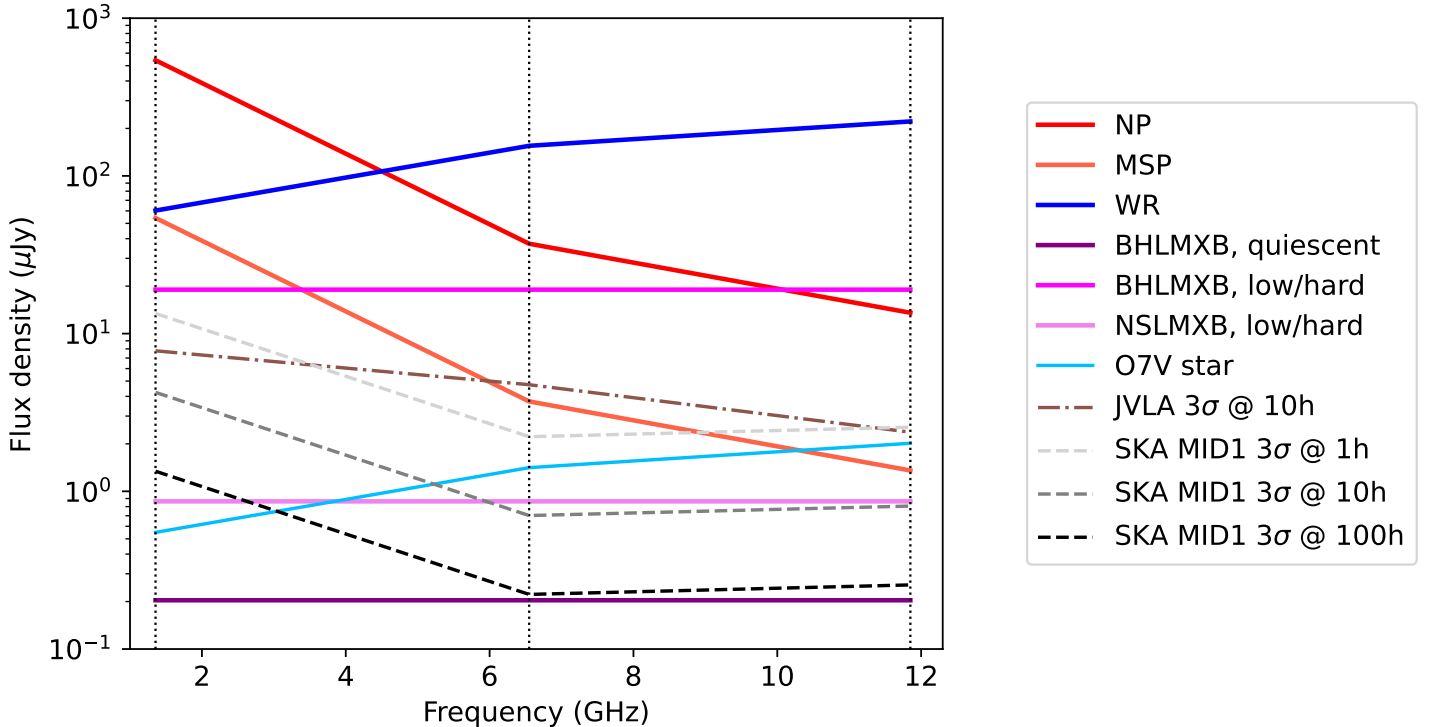


Figure 4: Flux densities of different types of radio point sources that we can expect to detect at the GC (solid lines). Vertical dotted lines indicate the central frequencies of bands 2 (1.355 GHz), 5a (6.55 GHz), and 5b (11.85 GHz). The dashed gray to black lines indicate the  $3\sigma$  rms of SKA1-Mid for integration times of 1 h, 10 h, and 100 h. The dash-dotted brown line indicates the  $3\sigma$  rms of the current JVLA. A GC distance of 8.25 kpc was assumed (Gravity Collaboration et al. 2020). NP: Normal pulsar, assuming a mean flux density of  $50 \mu\text{Jy}$  at 5 GHz and a spectral index of  $-1.7$  (Zhao et al. 2020). MSP: Millisecond pulsar, assuming a mean flux density of  $5 \mu\text{Jy}$  at 5 GHz and a spectral index of  $-1.7$  (Zhao et al. 2020). WR: Wolf Rayet star, assuming a flux density of  $200 \mu\text{Jy}$  at 10 GHz and a spectral index of 0.6 (Gallego-Calvente et al. 2021). O7V star: Thermal wind from an O7V star (approximately  $30 M_{\odot}$ ) assuming a mass loss rate of  $1 \times 10^{-7} M_{\odot}\text{yr}^{-1}$ , based on a MIST version 1.2 isochrone with solar metallicity and assuming a thermal spectral index of 0.6. BHLMXB quiescent: Here we have used the observed flux density of the quiescent BHLMXB XTE J1118+480, observed by Gallo et al. (2014), scaling it to the distance of the GC and assuming a flat spectral index. BHLMXB, low/hard: BH low mass X-ray binary in low/hard state, assuming a flat spectral index and a radio/X-ray luminosity of  $10^{28} \text{erg s}^{-1}/10^{34} \text{erg s}^{-1}$ . These fluxes correspond to the faintest detections given in Gallo et al. (2018), i.e. we expect most sources to be brighter. NSLMXB, low/hard: NSLMXB in low/hard state, assuming that NSLMXBs are about 22 times less radio loud than BHLMXBs (Gallo et al. 2018). As for BHLMXBs, this is a lower limit.

and may become available for a significant fraction of the GC in the next years (?). Also, specific fields may be observed with adaptive optics assisted near-infrared instruments on large ground-based telescopes, such as ERIS/VLT.

## 7 Survey requirements and possible setup

We propose to study the GC with a survey that covers three aspects: (1) covering a wide field that encompasses the entire CMZ; (2) aiming at the highest sensitivity in the most extreme region in the GC, the NSC, that surrounds the massive BH and probably contains a very high concentration of stellar remnants in the density cusp around the latter (e.g. Baumgardt et al. 2018); (3) studying the time domain by repeated observations of fields in the NSC and NSD to constrain properties of stellar remnants, such as the recurrence time between LMXB outbursts, and massive stars, such as the variability of their winds, and to measure the proper motion of the point sources.

Multi-wavelength observations will be necessary because spectral indices provide us with insight into the nature of the radio emission and therefore of the observed sources. The SKA GC survey should be carried out at frequencies of 1.4, 6.7, and 12.5 GHz (bands 2, 5a, and 5b). The angular resolution at these frequencies will be  $0.6''$ ,  $0.13''$ , and  $0.07''$ , respectively. This means that at the highest frequency and with a ten-year time baseline the proper motions of point sources detected at  $10\sigma$  can be measured with a precision of  $1 \text{mas yr}^{-1}$ . The proper motions will serve to constrain to which stellar structure a source pertains (e.g., see Shahzamanian et al. 2022) and how deep it is inside the gravitational potential at the GC. In addition, polarisation measurements will be crucial to distinguish non-thermal sources as NSs or BHs from other stars or

thermal sources. Figure 4 shows the flux densities expected from different objects of interest as a function of distance from Earth.

We assume an effective FWHM of the SKA1-Mid field-of-view of  $2.6'$  at 12.5 GHz. Assuming 1 h observations per pointing, we can cover a  $2.0^\circ \times 0.4^\circ$  field oriented parallel to the Galactic Plane and centred on Sgr A\* in 234 h, as is shown in Fig. 5. Additionally, several comparison fields should be observed in the inner Galactic Bulge so that we can assess the number and nature of sources that may overlap along the line of sight with the GC. We expect a relatively homogeneous source population at higher latitudes (mostly radio galaxies), therefore we estimate that four fields should be sufficient (4 h per field and per band). This results in a time requirement of 250 h. Due to the larger field-of-view at the lower frequencies, the same field can be covered in about 70 h at 6.7 GHz and 5 h at 1.4 GHz. In total, we will require 325 h for a GC survey that reaches an rms noise in the the continuum images of 2.0, 1.3, and  $1.2 \mu\text{Jy beam}^{-1}$  at 1.4, 6.7, and 12.5 GHz, respectively. For the line images, the expected rms noise level will be 140, 90 and  $85 \mu\text{Jy beam}^{-1}$ , respectively.

This shallow survey should be complemented by repeated deep observations of the NSC. We propose to observe the NSC with single 10 h pointings in bands 5a and 5b. The sensitivity reached for each 10 h pointing will be of 0.22 and  $0.26 \mu\text{Jy beam}^{-1}$  at 6.7, and 12.5 GHz. These observations should be repeated at 30 different epochs over several years to allow us to observe variability and proper motions and to be able – through stacking of the data – to reach a sensitivity sufficient to detect quiescent XBs at  $> 5\sigma$  in band 5. The time requirement for the NSC study will thus be 600 h. In conclusion, we propose to invest roughly 925 h for observing the arguably most interesting environment of the Milky Way with SKA1-Mid.

## Acronyms

BH	Black Hole	MSP	Millisecond Pulsar
CMZ	Central Molecular Zone	NS	Neutron Star
GC	Galactic Centre	NSC	Nuclear Star Cluster
GR	General Relativity	NSD	Nuclear Stellar Disc
IMBH	Intermediate Mass Black Hole	Sgr A*	Sagittarius A*
IMF	Initial Mass Function	SKA	Square Kilometre Array
ISM	Interstellar Medium	SMBH	Supermassive Black hole
LMXB	Low Mass X-ray Binary	XB	X-ray binary

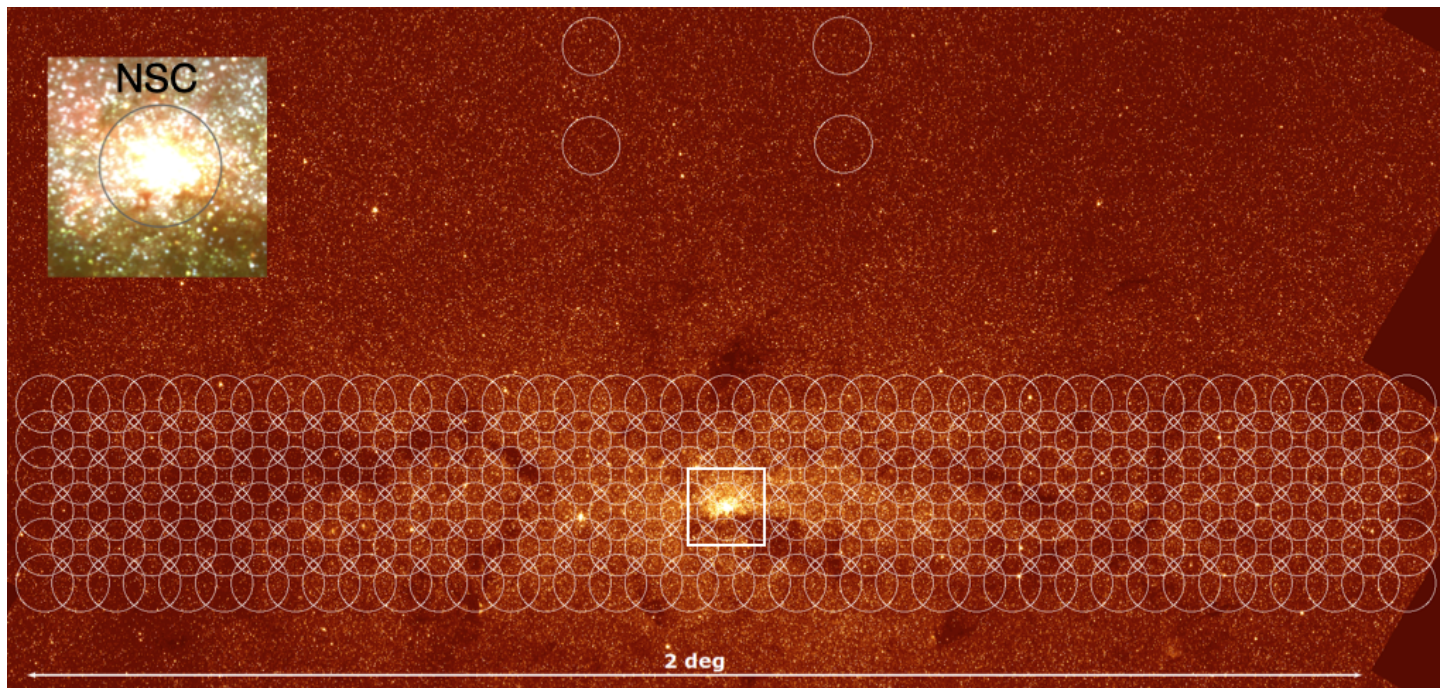


Figure 5: Possible layout of pointings at 12.5 GHz, overlaid over a Spitzer  $3.6 \mu\text{m}$  image. Galactic north is up, Galactic east is to the left. The NSC is shown in the zoomed inlet, with the 12.5 GHz beam overplotted. The four disconnected circles to the Galactic north are the comparison fields.

## Acknowledgments

RS, AA, AG, MPT, JM, LVM, and SSE acknowledge the Spanish Prototype of an SRC (SPSRC) service and support funded by the Ministerio de Ciencia, Innovación y Universidades (MICIU), by the Junta de Andalucía, by the European Regional Development Funds (ERDF) and by the European Union NextGenerationEU/PRTR. The SPSRC acknowledges financial support from the Agencia Estatal de Investigación (AEI) through the "Center of Excellence Severo Ochoa" award to the Instituto de Astrofísica de Andalucía (IAA-CSIC) (SEV-2017-0709) and from the grant CEX2021-001131-S funded by MICIU/AEI/ 10.13039/501100011033.

## References

- Abazajian, K. N. 2011, *J. Cosmology Astropart. Phys.*, 2011, 010
- Alexander, T. 2017, *ARA&A*, 55, 17
- Bartko, H., Martins, F., Trippe, S., et al. 2010, *ApJ*, 708, 834
- Baumgardt, H., Amaro-Seoane, P., & Schödel, R. 2018, *A&A*, 609, A28
- Bianchi, E., Remijan, A., Codella, C., et al. 2023, *ApJ*, 944, 208
- Bittner, A., Sánchez-Blázquez, P., Gadotti, D. A., et al. 2020, *A&A*, 643, A65
- Bland-Hawthorn, J. & Gerhard, O. 2016, *ARA&A*, 54, 529
- Bower, G. C., Deller, A., Demorest, P., et al. 2014, *ApJ*, 780, L2
- Bower, G. C., Deller, A., Demorest, P., et al. 2015, *ApJ*, 798, 120
- Clark, J. S., Lohr, M. E., Najarro, F., Dong, H., & Martins, F. 2018, *A&A*, 617, A65
- Clark, J. S., Patrick, L. R., Najarro, F., Evans, C. J., & Lohr, M. 2021, *A&A*, 649, A43
- Corbel, S., Coriat, M., Brocksopp, C., et al. 2013, *MNRAS*, 428, 2500
- Corbel, S., Miller-Jones, J. C. A., Fender, R., et al. 2015, in *Advancing Astrophysics with the Square Kilometre Array (AASKA14)*, 53
- Coriat, M., Corbel, S., Buxton, M. M., et al. 2009, *MNRAS*, 400, 123
- de Vicente, P., Martín-Pintado, J., Neri, R., & Colom, P. 2000, *A&A*, 361, 1058
- Degenaar, N., Wijnands, R., Cackett, E. M., et al. 2012, *A&A*, 545, A49
- Degenaar, N., Wijnands, R., Miller, J. M., et al. 2015, *Journal of High Energy Astrophysics*, 7, 137
- Deneva, J. S., Cordes, J. M., & Lazio, T. J. W. 2009, *ApJ*, 702, L177
- Dexter, J. & O’Leary, R. M. 2014, *ApJ*, 783, L7
- Do, T., Hees, A., Ghez, A., et al. 2019, *Science*, 365, 664
- Dong, H., Wang, Q. D., Cotera, A., et al. 2011, *MNRAS*, 417, 114
- Eatough, R., Lazio, T. J. W., Casanellas, J., et al. 2015, in *Advancing Astrophysics with the Square Kilometre Array (AASKA14)*, 45
- Feldmeier-Krause, A., Zhu, L., Neumayer, N., et al. 2017, *MNRAS*, 466, 4040
- Fender, R. P., Belloni, T. M., & Gallo, E. 2004, *MNRAS*, 355, 1105
- Fritz, T. K., Gillessen, S., Dodds-Eden, K., et al. 2011, *ApJ*, 737, 73
- Gadotti, D. A., Bittner, A., Falcón-Barroso, J., et al. 2020, *A&A*, 643, A14
- Gadotti, D. A., Sánchez-Blázquez, P., Falcón-Barroso, J., et al. 2019, *MNRAS*, 482, 506
- Gallego-Calvente, A. T., Schödel, R., Alberdi, A., et al. 2021, *A&A*, 647, A110
- Gallego-Calvente, A. T., Schödel, R., Alberdi, A., et al. 2022, *A&A*, 664, A49

Gallego-Cano, E., Schödel, R., Nogueras-Lara, F., et al. 2020, *A&A*, 634, A71

Gallo, E., Degenaar, N., & van den Eijnden, J. 2018, *MNRAS*, 478, L132

Gallo, E., Miller-Jones, J. C. A., Russell, D. M., et al. 2014, *MNRAS*, 445, 290

Garay, G. & Lizano, S. 1999, *PASP*, 111, 1049

Generozov, A., Stone, N. C., Metzger, B. D., & Ostriker, J. P. 2018, *MNRAS*

Genzel, R., Eisenhauer, F., & Gillessen, S. 2010, *Reviews of Modern Physics*, 82, 3121

Gravity Collaboration, Abuter, R., Amorim, A., et al. 2018, *A&A*, 615, L15

Gravity Collaboration, Abuter, R., Amorim, A., et al. 2020, *A&A*, 636, L5

Hailey, C. J., Mori, K., Bauer, F. E., et al. 2018, *Nature*, 556, 70

Henshaw, J. D., Barnes, A. T., Battersby, C., et al. 2023, in *Astronomical Society of the Pacific Conference Series*, Vol. 534, *Protostars and Planets VII*, ed. S. Inutsuka, Y. Aikawa, T. Muto, K. Tomida, & M. Tamura, 83

Heywood, I., Camilo, F., Cotton, W. D., et al. 2019, *Nature*, 573, 235

Heywood, I., Rammala, I., Camilo, F., et al. 2022, arXiv e-prints, arXiv:2201.10541

Hooper, D. & Goodenough, L. 2011, *Physics Letters B*, 697, 412

Hosek, Matthew W., J., Lu, J. R., Anderson, J., et al. 2019, *ApJ*, 870, 44

Hosek, Matthew W., J., Lu, J. R., Lam, C. Y., et al. 2020, *AJ*, 160, 143

Hußmann, B., Stolte, A., Brandner, W., Gennaro, M., & Liermann, A. 2012, *A&A*, 540, A57

Indriolo, N. & McCall, B. J. 2012, *ApJ*, 745, 91

Jankowski, F., van Straten, W., Keane, E. F., et al. 2018, *MNRAS*, 473, 4436

Jiménez-Serra, I., Martín-Pintado, J., Insausti, A., et al. 2022a, *Frontiers in Astronomy and Space Sciences*, 9, 843766

Jiménez-Serra, I., Martín-Pintado, J., Rivilla, V. M., et al. 2020, *Astrobiology*, 20, 1048

Jiménez-Serra, I., Rodríguez-Almeida, L. F., Martín-Pintado, J., et al. 2022b, *A&A*, 663, A181

Kim, S. S., Figer, D. F., Lee, H. M., & Morris, M. 2000, *ApJ*, 545, 301

Kim, S. S., Morris, M., & Lee, H. M. 1999, *ApJ*, 525, 228

Kormendy, J. & Ho, L. C. 2013, *ARA&A*, 51, 511

Kramer, M. 2016, *International Journal of Modern Physics D*, 25, 1630029

Kramer, M., Backer, D. C., Cordes, J. M., et al. 2004, *New A Rev.*, 48, 993

Kruijssen, J. M. D. & Longmore, S. N. 2013, *MNRAS*, 435, 2598

Kruijssen, J. M. D., Longmore, S. N., Elmegreen, B. G., et al. 2014, *MNRAS*, 440, 3370

Kruijssen, J. M. D., Pfeffer, J. L., Chevance, M., et al. 2020, *MNRAS*, 498, 2472

Lang, C. C., Johnson, K. E., Goss, W. M., & Rodríguez, L. F. 2005, *AJ*, 130, 2185

Launhardt, R., Zylka, R., & Mezger, P. G. 2002, *A&A*, 384, 112

Le Petit, F., Ruaud, M., Bron, E., et al. 2016, *A&A*, 585, A105

Leitherer, C., Chapman, J. M., & Koribalski, B. 1997, *ApJ*, 481, 898

Levy, R. C., Bolatto, A. D., Leroy, A. K., et al. 2022, *ApJ*, 935, 19

Liu, K., Wex, N., Kramer, M., Cordes, J. M., & Lazio, T. J. W. 2012, *ApJ*, 747, 1

Lower, M. E., Dai, S., & Johnston, S. 2024, arXiv e-prints, arXiv:2404.09098

Lu, J. R., Do, T., Ghez, A. M., et al. 2013, *ApJ*, 764, 155

Maccarone, T. J., Degenaar, N., Tetarenko, B. E., et al. 2022, *MNRAS*, 512, 2365

Martín, S., Mangum, J. G., Harada, N., et al. 2021, *A&A*, 656, A46

Martín-Pintado, J., Jiménez-Serra, I., Rodríguez-Franco, A., Martín, S., & Thum, C. 2005, *ApJ*, 628, L61

Matsunaga, N., Kawadu, T., Nishiyama, S., et al. 2011, *Nature*, 477, 188

Mauerhan, J. C., Munro, M. P., Morris, M. R., Stolovy, S. R., & Cotera, A. 2010, *ApJ*, 710, 706

Morris, M. 1993, *ApJ*, 408, 496

Munro, M. P., Pfahl, E., Baganoff, F. K., et al. 2005, *ApJ*, 622, L113

Nandakumar, G., Ryde, N., Schultheis, M., et al. 2018, *MNRAS*, 478, 4374

Neumayer, N., Seth, A., & Böker, T. 2020, *A&A Rev.*, 28, 4

Nogueras-Lara, F. 2022, *A&A*, 666, A72

Nogueras-Lara, F., Feldmeier-Krause, A., Schödel, R., et al. 2023, *A&A*, 680, A75

Nogueras-Lara, F., Gallego-Calvente, A. T., Dong, H., et al. 2018, *A&A*, 610, A83

Nogueras-Lara, F., Schödel, R., Gallego-Calvente, A. T., et al. 2019, *A&A*, 631, A20

Nogueras-Lara, F., Schödel, R., Gallego-Calvente, A. T., et al. 2020a, *Nature Astronomy*, 4, 377

Nogueras-Lara, F., Schödel, R., & Neumayer, N. 2021, *A&A*, 653, A133

Nogueras-Lara, F., Schödel, R., & Neumayer, N. 2022, *Nature Astronomy*, 6, 1178

Nogueras-Lara, F., Schödel, R., Neumayer, N., et al. 2020b, *A&A*, 641, A141

Oka, T., Geballe, T. R., Goto, M., Usuda, T., & McCall, B. J. 2005, *ApJ*, 632, 882

Pfuhl, O., Fritz, T. K., Zilka, M., et al. 2011, *ApJ*, 741, 108

Portegies Zwart, S. F., Makino, J., McMillan, S. L. W., & Hut, P. 2002, *ApJ*, 565, 265

Psaltis, D., Wex, N., & Kramer, M. 2016, *ApJ*, 818, 121

Ramatsoku, M., Murgia, M., Vacca, V., et al. 2020, *A&A*, 636, L1

Reid, M. J., Menten, K. M., Brunthaler, A., et al. 2014, *ApJ*, 783, 130

Requena-Torres, M. A., Martín-Pintado, J., Martín, S., & Morris, M. R. 2008, *ApJ*, 672, 352

Rich, R. M., Ryde, N., Thorsbro, B., et al. 2017, *AJ*, 154, 239

Rivilla, V. M., Colzi, L., Jiménez-Serra, I., et al. 2022, *ApJ*, 929, L11

Rivilla, V. M., Jiménez-Serra, I., García de la Concepción, J., et al. 2021, *MNRAS*, 506, L79

Rivilla, V. M., Sanz-Novo, M., Jiménez-Serra, I., et al. 2023, *ApJ*, 953, L20

Rodríguez-Almeida, L. F., Jiménez-Serra, I., Rivilla, V. M., et al. 2021a, *ApJ*, 912, L11

Rodríguez-Almeida, L. F., Rivilla, V. M., Jiménez-Serra, I., et al. 2021b, *A&A*, 654, L1

Rudnick, L., Brüggén, M., Brunetti, G., et al. 2022, *ApJ*, 935, 168

Russell, D. M., Fender, R. P., Hynes, R. I., et al. 2006, *MNRAS*, 371, 1334

Russell, D. M., Fender, R. P., & Jonker, P. G. 2007, *MNRAS*, 379, 1108

Sakamoto, K., Mao, R.-Q., Matsushita, S., et al. 2011, *ApJ*, 735, 19

Salati, P. 2014, in *International Journal of Modern Physics Conference Series*, Vol. 30, *International Journal of Modern Physics Conference Series*, 1460256

Sanders, J. L., Matsunaga, N., Kawata, D., et al. 2022, MNRAS, 517, 257

Sanz-Novo, M., Rivilla, V. M., Jiménez-Serra, I., et al. 2023, ApJ, 954, 3

Schnitzeler, D. H. F. M., Eatough, R. P., Ferrière, K., et al. 2016, MNRAS, 459, 3005

Schödel, R., Feldmeier, A., Kunneriath, D., et al. 2014a, A&A, 566, A47

Schödel, R., Feldmeier, A., Neumayer, N., Meyer, L., & Yelda, S. 2014b, Classical and Quantum Gravity, 31, 244007

Schödel, R., Nogueras-Lara, F., Gallego-Cano, E., et al. 2020, A&A, 641, A102

Schoedel, R., Longmore, S., Henshaw, J., et al. 2023, arXiv e-prints, arXiv:2310.11912

Schönrich, R., Aumer, M., & Sale, S. E. 2015, ApJ, 812, L21

Schultheis, M., Fritz, T. K., Nandakumar, G., et al. 2021, A&A, 650, A191

Schultheis, M., Rich, R. M., Origlia, L., et al. 2019, A&A, 627, A152

Scoville, N. Z., Stolovy, S. R., Rieke, M., Christopher, M., & Yusef-Zadeh, F. 2003, ApJ, 594, 294

Shahzamanian, B., Schödel, R., Nogueras-Lara, F., et al. 2022, A&A, 662, A11

Sobey, C., Bassa, C. G., O’Sullivan, S. P., et al. 2022, A&A, 661, A87

Sormani, M. C., Magorrian, J., Nogueras-Lara, F., et al. 2020, MNRAS, 499, 7

Sormani, M. C., Sanders, J. L., Fritz, T. K., et al. 2022, MNRAS, 512, 1857

Spitler, L. G., Lee, K. J., Eatough, R. P., et al. 2014, ApJ, 780, L3

Torne, P., Desvignes, G., Eatough, R. P., et al. 2021, A&A, 650, A95

Tsuboi, M., Kitamura, Y., Tsutsumi, T., et al. 2017, ApJ, 850, L5

Viti, S., Collings, M. P., Dever, J. W., McCoustra, M. R. S., & Williams, D. A. 2004, MNRAS, 354, 1141

Voss, R. & Gilfanov, M. 2007, MNRAS, 380, 1685

Wongphechauxsorn, J., Champion, D. J., Bailes, M., et al. 2024, MNRAS, 527, 3208

Yusef-Zadeh, F., Arendt, R. G., Wardle, M., & Heywood, I. 2023, ApJ, 949, L31

Yusef-Zadeh, F., Morris, M., & Chance, D. 1984, Nature, 310, 557

Yusef-Zadeh, F. & Wardle, M. 2019, MNRAS, 490, L1

Yusef-Zadeh, F., Zhao, J.-H., Arendt, R., et al. 2024, MNRAS, 530, 254

Zeng, S., Jiménez-Serra, I., Rivilla, V. M., et al. 2021, ApJ, 920, L27

Zhao, J.-H., Morris, M. R., & Goss, W. M. 2020, ApJ, 905, 173

Zhao, J.-H., Morris, M. R., & Goss, W. M. 2022, ApJ, 927, L6

Zhu, Z., Li, Z., & Morris, M. R. 2018, ApJS, 235, 26